Digest Journal of Nanomaterials and Biostructures Vol. 14, No. 4, October-December 2019, p. 855-866

TUNING OF STRUCTURAL, MAGNETIC AND OPTICAL PROPERTIES OF SILVER DOPED COBALT CHROMIUM FERRITE FERRITES THIN FILM BY PLD TECHNIQUE

T. ZEEHAN*, S. ANJUM, S. WASEEM, M. RIAZ, R. ZIA
Lahore Colleage For Women University Lahore Pakistan

The insertion of different elements in the cobalt ferrite spinel structure can significantly change the structural and magnetic characteristics of cobalt ferrite bulks and thin films. Pulsed Laser Deposition (PLD) is an extensively used method which permits the growth of thin films with complex chemical formula. The thin film of $Co_{1-x}Ag_xCr_{0.5}Fe_{1.5}O_4$ (x=0, 0.2, 0.4, 0.6, 0.8, 1.0) have been grown on single crystal p-type silicon Si(100) substrate by pulsed laser deposition technique using Nd-YAG laser. The structural properties of the thin films have been carried out by X-ray diffractrometer (XRD). The structural analyses confirm the epitaxial growth of (220) plane spinel ferrites with cubic symmetry. Surface morpholgy is deeply studied using Atomic Force Microscopy (AFM). The magnetic properties of deposite thin films have been measured by Vibrating Sample Magnetometer (VSM). The optical parameters like absorption, band gap energy and thickness of the thin films have been extracted from Spectroscopy Ellipsometry (SE).

(Received April 12, 2019; Accepted October 1, 2019)

Keywords: Magnrtic materials, Bond Length, Crystallite size, Refractive index

1. Introduction

The transition metal ferrites are the family of oxides which play a vital role in an extensive variety of fields, because of the variability of transition metal cations that may be merged into the lattice of the parent magnetite structure. In the case where these ferrites are used for catalytic, magnetic or electrical applications, they are prepared in the form of ceramics materials with very high density [1, 2],

With the progress of magnetic, magneto-optical memory and high-frequency devices of nano materials having small dimensions, there has been a substantial increase in the interest of ferrite thin film in current years. There are various applications of thin films of ferrite, such as humidity or gas sensors for which nano-sized materials are required[3] . The Properties of ferrite thin films are usually found to be changed from that of the bulk for several reasons such as grain boundaries, high defect density, crystallite size, limitations caused by substrate, texture and also depend on fabrication parameters [4, 5] [6].

The thin films of silver doped cobalt chromium ferrite can be obtained by various methods[7] [8, 9] [10] but the most auspicious practice to deposit the epitaxial thin films with privileged crystallographic direction and perpendicular magnetic anisotropy was establish to be Pulsed Laser Deposition (PLD)[10].

The magnetic properties depend on the induced anisotropy which is produced by comprehensive strain to the plan of thin film. Sometimes the films consist of small crystalline grains surrounded by thin region of amorphous material. Post deposition annealing improves the crystallinity of the films, at the same time reducing the field required for saturation. For Ni ferrite film was observed that the interlayer exchange coupling increases when the bilayer is annealed at temperatures below 600C^o[7] . For integrated planar circuits operating at high frequencies however, designs based on thin NiZn ferrite films are expected to have important applications[11]

*Corresponding author: talats@hotmail.com

The oxygen pressure during growth affects the unit cell volume and stress of the film[12]. The Zn ferrite films, tough antiferromagnetic, are studied for application to magnetic devices, particularly the optical magnetic memory devices. Izaki et al. [13] [prepared Fe_3O_4 film at low temperature by immersing a Pd/Ag-catalyzed substrate in aqueous iron nitrate and di-methylamine borne complex (DMAB) solution.

This study was focused on the structural, magnetic and optical characterization of silver doped cobalt chromium ferrite thin films. To our knowledge, results on silver doped cobalt chromium ferrite thin films cobalt ferrite thin films deposited by PLD technique were not reported until now. The aim of this work was to focus on the structural, magnetic and optical characterization of silver doped cobalt chromium ferrite thin

2. Experimental procedure

A thin film of $Ag_xCO_{1-x}Cr_{0.5}Fe_{1.5}O_4$ magnetic materials with different composition has been deposited on Si (100) substrate. A schematic diagram of the experimental setup is shown in Figure. The ablation of each target was done by Nd-YAG laser with wave length of 232nm(second harmonic) at a fluence of 2.5 J/cm^2 and operated at a repetition rate of 20 Hz. The base pressure in the chamber was ~ 10^{-4} Torr which was attained by rotary pump. An optimized distance between substrate and target is 1.5cm. The rotation of target was done by using a programmable motor mounted at 6 rpm. The irradiation of each target was done with 5000 number of shots and the substrate temperature is also kept constant in each case i.e 300K^0.

After the fabrication of bulk ferrites and their thin film deposition, these materials were characterized for their structural, magnetic, optical and evaluation.

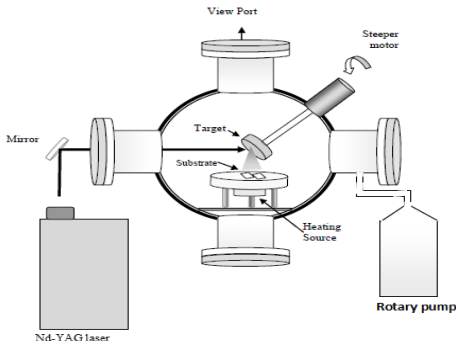

Fig. 1. A schematic of the experimental setup for PLD.

3. X-Ray diffractometer

The comparative 'XRD' patterns of Co_{1-x} Ag_x $Cr_{0.5}$ $Fe_{1.5}$ O_4 thin films, where (x=0, 0.2, 0.4, 0.6, 0.8, 1.0) are shown in figure 1. This diffractrometr graph revealed that at x=0 the most intense peak (311) of the cubic symmetry is not present in the spectra, but as the concentration of Ag increases this plane appeared slightly. The reason of absence of (311) plane at low concentration is that XRD study is out of plane measurement which identify simply those planes that lies perpendicular to the sample surface. In these samples (311) plane lies parallel to the surface or in plane that is why the reflection of this peak is not observed.

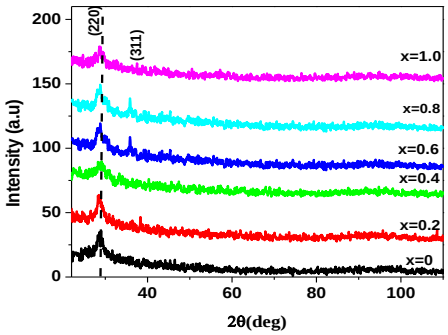

Fig. 2. XRD patterns for the thin film of $Co_{1-x}Ag_xCr_{0.5}Fe_{1.5}O_4$.

It has been revealed from the pattern that peaks at (220) and (311) planes shifted towards the decreasing two theta angles that are possibly due to structural difference of substrate and thin film. The lattice parameters for cubic symmetry have been intended from the major peak (220) using equation 1[14, 15]:

$$a = d\,(h2+k2+l2) \quad (1)$$

The crystallite size has been evaluated by calculating the FWHM of most intense peak (220) using the formula 2 [16]:

$$D_p = 0.9\lambda/\beta\cos\theta \quad (2)$$

The parameters extracted form XDR are listed in Table 1. The variation of lattice parameters and crystallite size as a function of silver contents has been shown in Fig. 3.

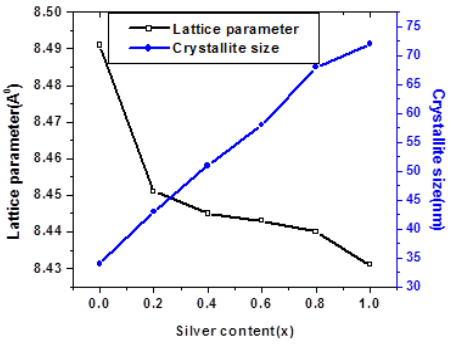

Fig. 3. Variation of lattice parameters and crystallite of $Co_{1-x}Ag_xCr_{0.5}Fe_{1.5}O_4$ thin film.

It is observed from the figure that lattice parameters decreases with increasing the silver concentration which is due to the greater ionic radius of the silver ion than the cobalt ion that establishes the internal strains inside the material. The values of lattice constants in target ferrites in the range of 8.297A^0 to 8.265 A^0 but in case of their thin films are 8.491 A^0 to 8.431A^0 which shows the presence of larger lattice strain.

The analysis revealed that the crystallite size increases with increasing the silver contents. This trend can be explained as follows, when heat is provided to the substrate during the deposition the thermal expansion cause lattice mismatch that can induces the internal stresses so that the defects in the films are induced and thin films become less crystalline and as a result the crystallite size increases. The hopping lengths L_A and L_B are evaluated by the formulas their values have been listed in Table 2 [17]:

$$LA = a\sqrt{3}/4 \quad (3)$$

$$LB = a\sqrt{2}/4 \quad (4)$$

It is reveled from Fig. 4 that the hopping length decreases with increasing the silver concentration. As L_A and L_B are directly dependent on lattice parameter, so the squeezing of hopping lengths is due to reduction of lattice parameters with enrichment of silver contents.

Table 1. Parameters extracted from XRD from thin film of $Co_{1-x}Ag_xCr_{0.5}Fe_{1.5}O_4$.

Silver Contents (x)	d –spacing (nm)	Lattice parameter (A^0)	Crystallite size x(nm)	Band gap energy (eV)
0	3.011	8.491	34	3.07
0.2	2.997	8.451	43	3.1
0.4	2.995	8.445	51	2.9
0.6	2.994	8.443	58	2.56
0.8	2.993	8.440	68	1.8
1.0	2.990	8.431	72	--

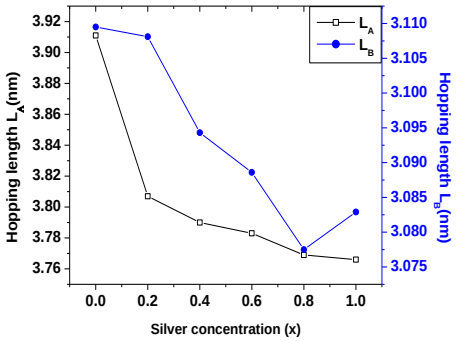

Fig. 4. Variation of hopping lengths with silver concentration in $Co_{1-x}Ag_xCr_{0.5}Fe_{1.5}O_4$ thin film.

Table 2. Parameters extracted from FTIR from thin film of $Co_{1-x}Ag_xCr_{0.5}Fe_{1.5}O_4$.

Silver content(x)	L_A(nm)	L_B(nm)
$Co_{1.0}Cr_{0.5}Fe_{1.5}O_4$	3.911	3.1095
$Co_{0.8}Ag_{0.2}Cr_{0.5}Fe_{1.5}O_4$	3.807	3.1081
$Co_{0.6}Ag_{0.4}Cr_{0.5}Fe_{1.5}O_4$	3.790	3.0943
$Co_{0.4}Ag_{0.6}Cr_{0.5}Fe_{1.5}O_4$	3.783	3.0886
$Co_{0.2}Ag_{0.8}Cr_{0.5}Fe_{1.5}O_4$	3.769	3.0775
$Ag_{1.0}Cr_{0.5}Fe_{1.5}O_4$	3.766	3.0829

3.1. AFM analysis

The AFM images of thin films have been shown in Fig. 5. The change in color over the vertical scale shows the variation in thickness. The values estimated from 2D and 3D images of AFM are the average roughness, means grain size and root mean square values have been summarized in Table 3. The number of scans has been taken from different areas of the film to ensure the homogeneity of the thin films. At low concentration of Ag the aggregation of the particles are negligible and they are mono-dispersed. In the last two samples the mechanism of

splashing has been seen that forms the particulates with geometric order on the surface of film [18]. The estimated average particles sizes of all samples are tabulated in Table 3 which confirms nano-granular morphology are in the range of 13 to 59 nm. The average and root mean square roughness values are also increasing with increasing the silver contents which may be due to increasing grain size and thickness [19]. The grain size and roughness as determined from AFM are given in Table 1. Roughness determined by the Ellipsometry and AFM are approximately comparable.

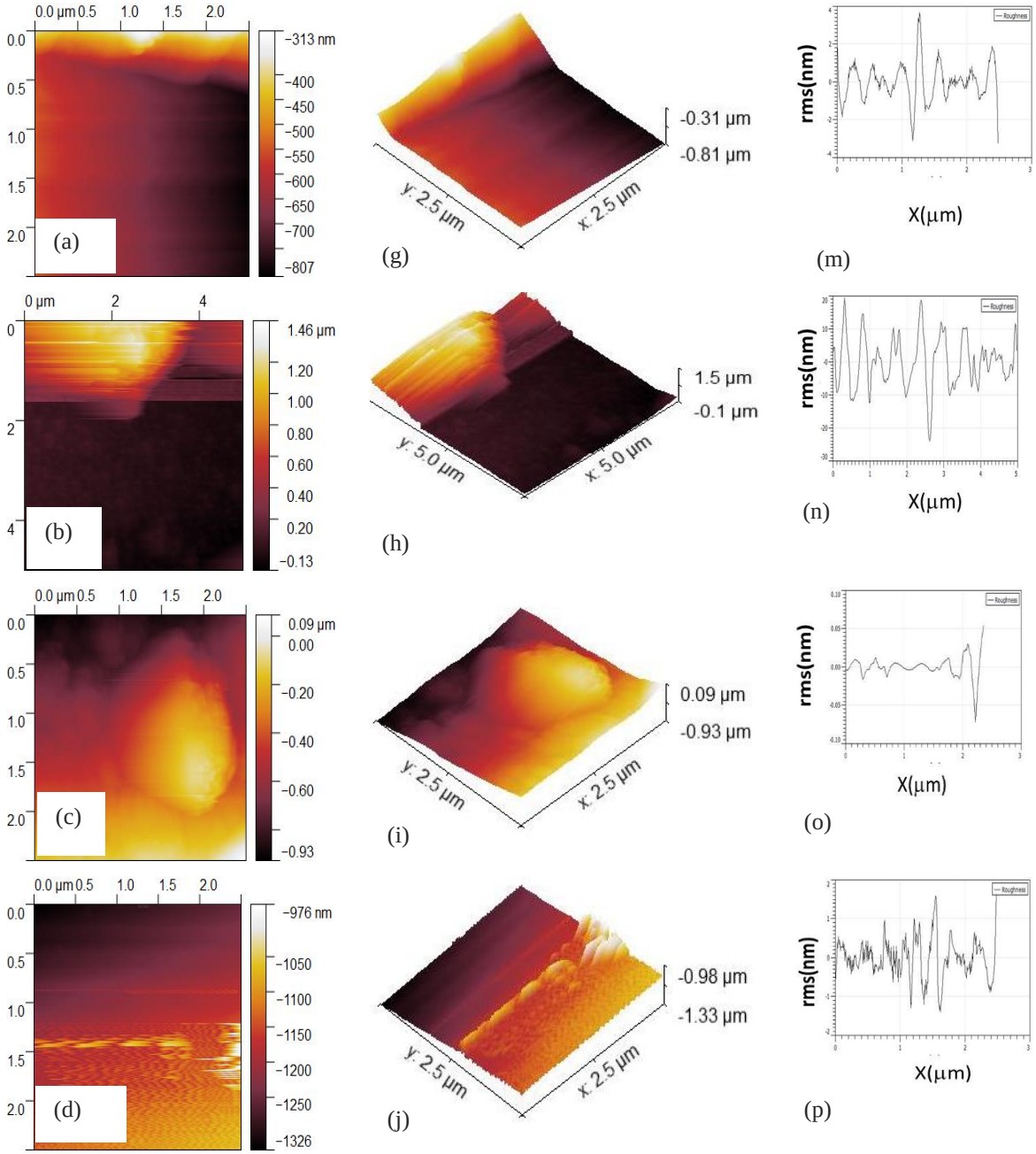

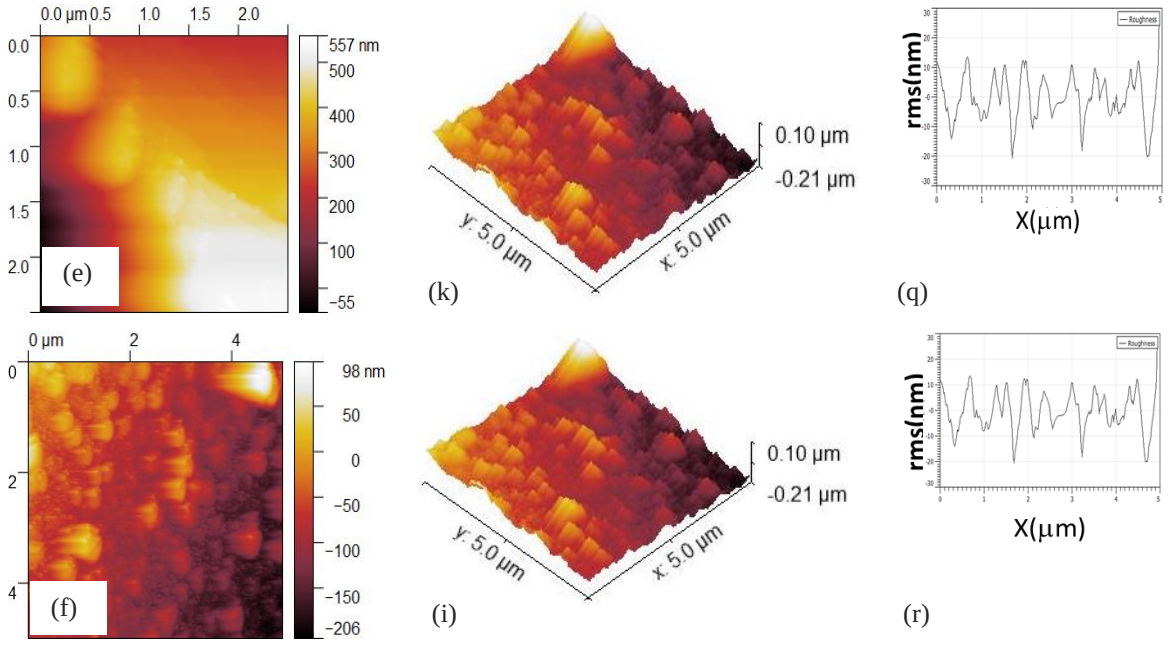

Fig. 5. AFM analysis of silver doped cobalt chromium ferrites thin film, 5(a,b,c,d,e,f) 2D analysis, 5 (g,h,i,j,h,l) 3D analysis and (m,n,o,pq,r) roughness profile.

Table 3. Average roughness, mean grain size and root mean square values of $Co_{1-x}Ag_xCr_{0.5}Fe_{1.5}O_4$ thin film.

Silver contents(x)	Average Roughness (nm)	Mean grain Size (nm)	Root mean square (nm)
0	6	13	8
0.2	0.7	17	0.5
0.4	2.0	23	1.0
0.6	0.4	24	2.6
0.8	6.0	36	7.5
1.0	8.6	59	14

3.1.1. Optical properties

The optical properties of the deposited thin films have been analyzed by spectroscopy ellipsometery. The parameters extracted from the ellipsometric data are refractive index, absorption, reflection and band gap energies that play a significant role in devices designing for the spectral dispersion, optical device performance and optical communication.

The Cauchy model is fitted to the ellipsometric data in visible spectral range to avoid the correlation with constants for calculation of the different parameters. The refractive index as a function of wavelength is plotted in Fig. 6. It is observed from figure that enhancement of Ag doping decreases the value of refractive index especially in the region of 500 to 700 nm. The refractive index of thin film at 450 nm wavelength is 0.061. 0.10.0.11, 0.12 and 0.13 for (x= 0.2, 0.4, 0.6, 0.8 and 1.0) respectively.

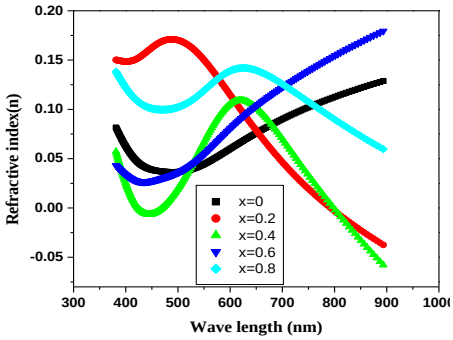

Fig. 6. The variation of refractive index with silver contents in $Co_{1-x}Ag_xCr_{0.5}Fe_{1.5}O_4$ thin film.

The reflectance and absorbance of the thin films can be calculated by the formulae [20]:

$$R= [(n-1)^2+k^2]/ [(n+1)^2+k^2] \quad (5)$$

$$A= 4n/[(n+1)^2+k^2] \quad (6)$$

It has been observed from Fig. (7 and 8) that the absorbance decreases and reflectance increases with increasing the silver contents which is due to the highly reflecting nature of the silver. It has been observed from the table that thickness increases with increasing silver ions. So, that the enhancement in absorption and reduction in reflection is in wavelength range of 450 to 750 nm is attributed to increase in thickness.

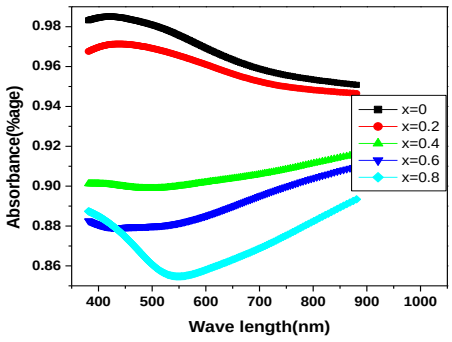

Fig. 7. Comparison of absorbance of $Co_{1-x}Ag_xCr_{0.5}Fe_{1.5}O_4$ thin film.

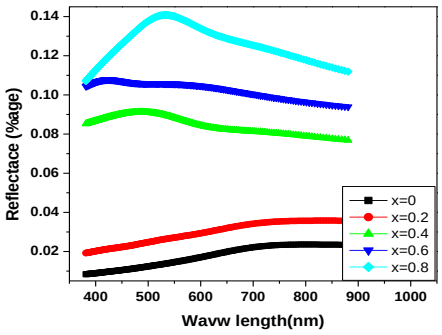

Fig. 8. Comparison of reflectance of $Co_{1-x}Ag_xCr_{0.5}Fe_{1.5}O_4$ thin film.

The values of optical band gap energy for thin films with different concentrations of silver can be intended as follows [21]:

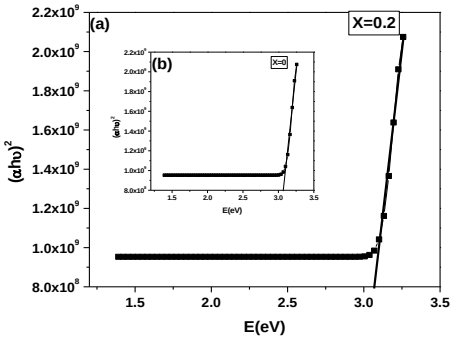

Fig. 9(a). Band gap energy with silver concentration of $Co_{1-x}Ag_xCr_{0.5}Fe_{1.5}O_4$ thin film (a): at x=0.2, (b): inset at x=0.

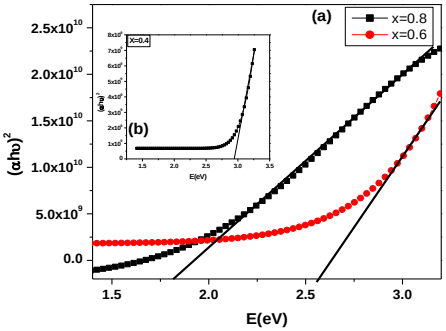

Fig. 10(b). Band gap energy of $Co_{1-x}Ag_xCr_{0.5}Fe_{1.5}O_4$ thin film (a): x=0.6, 0.8 and (b): inset is at x=0.4.

Table 4. Variation of optical band gap with different concentration of silver contents in $Co_{1-x}Ag_xCr_{0.5}Fe_{1.5}O_4$ thin film.

Silver contents (x)	**Thickness (nm)**	**Roughness (nm)**	**Energy band gap (eV)**
$Co_1Ag_0Cr_{0.5}Fe_{1.5}O_4$	130	32.8	3.07
$Co_{0.8}Ag_{0.2}Cr_{0.5}Fe_{1.5}O_4$	142	6.17	3.2
$Co_{0.6}Ag_{0.4}Cr_{0.5}Fe_{1.5}O_4$	261	9.42	2.9
$Co_{0.4}Ag_{0.6}Cr_{0.5}Fe_{1.5}O_4$	290	12.0	2.56
$Co_{0.2}Ag_{0.8}Cr_{0.5}Fe_{1.5}O_4$	300	49	1.8

The plot of $(\alpha h\upsilon)^2$ verses $h\upsilon$ has been shown in Fig. 10(a ,b). The band gap energy can be obtained by extra plotting the linear part to $(\alpha h\upsilon)^2 = 0$. Where "m" is the type of transition. If m=1/2 the allowed transition is direct otherwise if m=2 the indirect transition is allowed. The values of optical band gap observed from Fig. 10 (a,b) are listed in table 4.

It has been observed from the Fig. 11 that the band gap energy reduces with addition of silver concentration. That may be due to increase in adhesion between deposited material and hot substrate that leads to increase in grain size and thickness with increasing the silver that is responsible for the narrowing the band gap energy in the film [22].

The narrowing of band gap may be explained as: that the unsaturated bonds are formed during the deposition which causes the insufficient number of atoms. These bonds are responsible for the formation defects which create the localized states in thin film. So as the films become

thick, greater the width of the localized states in the band gap. As a result the optical band gap decreases and consequently the reduction in band gap energy. Furthermore this decline in band gap by adding the silver contents may be describe in term of electron dependence on band shift in the thin film. The optical band gap is associated with the electron transition from valance band to the Fermi levels in conduction band for the semiconductor degeneration. According to the Moss Burstein effect the values of bands should increase with Ag doping but the band gap energy values decrease with Ag concentration. This may be explained in term of increasing defects like stresses, oxygen vacancies, impurities, incomplete replacement of dopant with host atom and amount of disorder [23] The relation between optical band gap and film thickness with different concentrations of silver have been shown in figure 4.58.

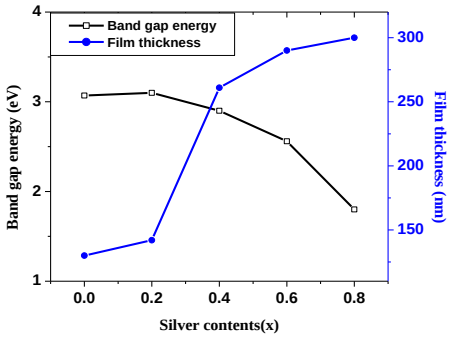

Fig. 11. The variation of band gap energy and film thickness as a function of silver contents in $Co_{1-x}Ag_xCr_{0.5}Fe_{1.5}O_4$ thin film.

The roughness decrease drastically for the silver doping concentration of (x=0 to x=0.6) and then increases. This trend of roughness profile in ellipsometric analysis is comparable with the AFM analysis. The increase in film thickness and decline in its corresponding root mean square (rms) values are has been observed from the table which is due to greater crystallite size. The reason of increasing thickness of film is also due to reduced stresses at film interface and substrate that help to grow the film in upward direction. At the doping concentration x=0.2 the band gap is 3.2 eV which is highest band gap energy which shows that the thin film becomes dielectric material and it has potential application in the optoelectronic devices [24].

3.1.2. Magnetic properties

The M-H loops of all thin films have been attained from VSM machine and their comparative plots are shown in Fig. 12. The estimated parameters like saturation magnetization, coercivity and remnant magnetization are extracted from the loops are listed in the Table 5.

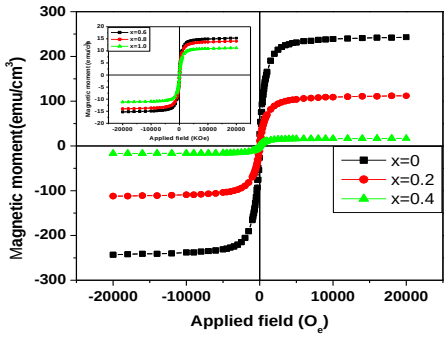

Fig. 12 Hysteresis loop of $Co_{1-x}Ag_xCr_{0.5}Fe_{1.5}O_4$ thin film.

Table 5. Parameters extracted from M-H loop of $Co_{1-x}Ag_xCr_{0.5}Fe_{1.5}O_4$.

Silver content(x)	Saturation magnetizationMs (emu/cc)	Coercivity Hc (kOe)	Remnant magnetization Mr (emu/cc)
$Co_1Ag_0Cr_{0.5}Fe_{1.5}O_4$	242	76	25
$Co_{0.8}Ag_{0.2}Cr_{0.5}Fe_{1.5}O_4$	110	74	11
$Co_{0.6}Ag_{0.4}Cr_{0.5}Fe_{1.5}O_4$	17	63	6.2
$Co_{0.4}Ag_{0.6}Cr_{0.5}Fe_{1.5}O_4$	15	51	2.1
$Co_{0.2}Ag_{0.8}Cr_{0.5}Fe_{1.5}O_4$	14	42	1.2
$Ag_{1.0}Cr_{0.5}Fe_{1.5}O_4$	12	47	0.9

It is observed Fig. 13 that saturation magnetization of the films decreases with the Ag concentration which may because of inadequate crystallization and non-magnetic nature of Ag. Actually by increasing the thickness of film the defects are produced in the thin films that lead to decrease the saturation magnetization.

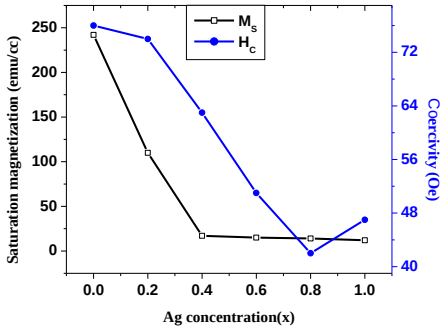

Fig. 13. Variation of saturation magnetization and coercivity as a function of silver in $Co_{1-x}Ag_xCr_{0.5}Fe_{1.5}O_4$ thin film.

In thin films it is very interesting result that the sample which has maximum concentration of Ag also shows the ferromagnetic behavior where as in bulk materials these materials are showing the paramagnetic behavior

It has been observed from the figure that value of coercivity decreases form 76Oe to 47Oe with increasing the silver concentration which may be due to increasing thickness of the films from 130 to300nm. Actually as the thickness increases the size of grains increases, which decrease the grain boundaries and consequently coercivity decrease [25]. Actually the process of magnetization due to movement of domain wall need low energy in comparison of domain rotation [26]. Hence the number of walls rises with the size of grains and the contribution due to the wall movement to magnetize and demagnetize increases. Though the samples have larger grains are expected to have low value of coercivity [27]. The variation of coercivity and film thickness with silver concentration is shown in Fig. 14.

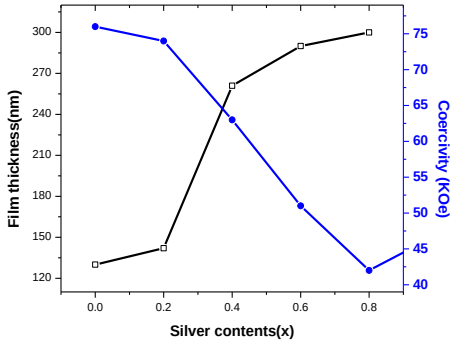

Fig. 14. Variation of film thickness and crystallite size with silver contents in $Co_{1-x}Ag_xCr_{0.5}Fe_{1.5}O_4$ *thin film.*

Furthermore the magnetic properties are also affected by anisotropy. The magnetic anisotropy is calculated by formula

$$K= H_C \times M_S/0.98 \quad (7)$$

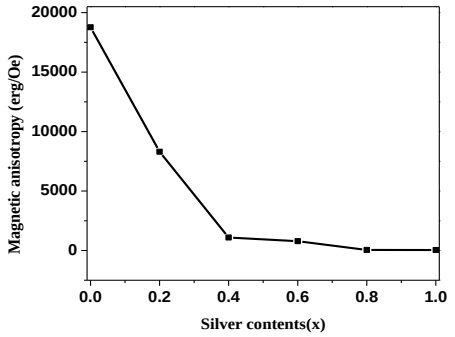

Fig. 15. Variation of magnetic anisotropy as a function of silve contents contents in $Co_{1-x}Ag_xCr_{0.5}Fe_{1.5}O_4$ *thin film.*

It is revealed from figure 15 that magnetic anisotropy in the films decreasing with silver addition that may be due to crystalline structure or texturing, stresses created during the film growth and grain size etc [28]. But there is no textured growth in the present deposited film therefore the anisotropy is not expected from magneto-crystalline. So the presence of stresses affects the overall domain structure and these stresses affect the shape and related parameters of hysteresis loop.

Conclusions

The film has no preferential orientation structurally, hence the easy axes (220) plane located randomly. Therefore it is concluded that magnetic properties of thin films does not depend upon the applied field direction. This results that the thin film is appropriate for isotropic recording application.

References

[1] R. Rennard, W. Kehl, Journal Of Catalysis **21**(3), 282 (1971).
[2] G. Dube, V. Darshane, Journal Of Molecular Catalysis **79**(1-3), 285 (1993).
[3] Y. Shimizu, M. Egashira, Mrs Bulletin **24**(6), 18 (1999).
[4] C. Xu, J. Tamaki, N. Miura, N. Yamazoe, Chemistry Letters **19**(3), 441 (1990).
[5] P. Rao, R. Godbole, D. Phase, R. Chikate, S. Bhagwat, Materials Chemistry And Physics **149**, 333 (2015).
[6] X. Sui, M. H. Kryder, Applied Physics Letters **63**(11), 1582 (1993).
[7] Y. Suzuki, R. Van Dover, E. Gyorgy, J. M. Phillips, V. Korenivski, D. Werder, C. Chen, R. Cava, J. Krajewski, W. Peck Jr, Applied Physics Letters **68**(5), 714 (1996).
[8] J. Yin, B. Liu, J. Ding, Y. Wang, Bulletin of Materials Science **29**(6), 573 (2006).
[9] F. Zhang, S. Kantake, Y. Kitamoto, M. Abe, IEEE Transactions On Magnetics **35**(5), 2751 (1999).
[10] P. Dorsey, P. Lubitz, D. Chrisey, J. Horwitz, Journal Of Applied Physics **79**(8), 6338 (1996).
[11] P. Dorsey, B. Rappoli, K. Grabowski, P. Lubitz, D. Chrisey, J. Horwitz, Journal Of Applied Physics **81**(10), 6884 (1997).
[12] C. Williams, D. Chrisey, P. Lubitz, K. Grabowski, C. Cotell, Journal Of Applied Physics **75**(3), 1676 (1994).
[13] M. Izaki, O. Shinoura, Advanced Materials **13**(2), 142 (2001).
[14] A. A. Hossain, T. Biswas, T. Yanagida, H. Tanaka, H. Tabata, T. Kawai, Mater. Chem. Phys. **120**(2), 461 (2010).
[15] X. Zhao, W. Wang, Y. Zhang, S. Wu, F. Li, J. P. Liu, Red. Chem. Eng. J **250**, 164 (2014).
[16] V. J. Hurst, P. A. Schroeder, R. W. Styron, Anal. Chim. Acta **337**(3), 233 (1997).
[17] P. Graves, C. Johnston, J. Campaniello, Mater. Res. Bull **23**(11), 1651 (1988).
[18] Q. Wei, J. Sankar, A. Sharma, Y. Yamagata, J. Narayan, J. Vac. Sci. Technol. **19**(1), 311 (2001).
[19] J. Islam, Y. Yamamoto, H. Hori, J. Magn. Magn. Mater. **310**(2), 2234 (2007).
[20] I. Smurov, Surf Coat Technol. **202**(18), 4496 (2008).
[21] S. Anjum, M. S. Rafique, M. Khaleeq-Ur-Rahman, K. Siraj, A. Usman, S. Hussain, S. Naseem, J. Magn. Magn. Mater. **324**(5). 711 (2012).
[22] C. Ramana, R. Smith, O. Hussain, Phys. Status Solidi A, **199**(1), (2003).
[23] K. Chen, F.-Y. Hung, S.-J. Chang, Z. Hu, Appl. Surf. Sci. **255**(12), 6308 (2009).
[24] G. Varughese, P. Jithin, K. Usha, Int. J. Phys. Sci. **5**(2), 146 (2015).
[25] N. Gupta, A. Verma, S. C. Kashyap, D. Dube, J. Magn. Magn. Mater. **308**(1), 137 (2007).
[26] M. Le Floc'h, A. Konn, Le Journal De Physique Iv, **7**(C1): C1-187-C1-190 (1997).
[27] A. Verma, T. Goel, R. Mendiratta, P. Kishan, J. Magn. Magn. Mater. **208**(1), 13 (2000).
[28] Y.-P. Zhao, R. Gamache, G.-C. Wang, T.-M. Lu, G. Palasantzas, J. T. M. De Hosson, J. Appl. Phys. **89**(2), 1325 (2001).